

The high energy emission of GRO J1655–40 as revealed with INTEGRAL spectroscopy of the 2005 outburst

M. D. Caballero-García¹, J. M. Miller², E. Kuulkers³, M. Díaz Trigo³, J. Homan⁴,
W. H. G. Lewin⁴, P. Kretschmar³, A. Domingo¹, J. M. Mas-Hesse⁵, R. Wijnands⁶, A. C.
Fabian⁷, R. P. Fender^{8,6}, M. van der Klis⁶

mcaballe@laeff.inta.es

ABSTRACT

We present broadband (3–500 keV) INTEGRAL X-ray spectra and X-ray/optical light curves of the luminous black hole X-ray transient and relativistic jet source GRO J1655–40. Our analysis covers four Target of Opportunity observations of the outburst that started in February 2005. We find that the high energy emission of GRO J1655–40 can be modelled well with an *unbroken* power-law (with photon indices of $\Gamma = 1.72 \pm 0.03, 2.21 \pm 0.04$ for the first and the second observations, respectively). These correspond to hard and thermal dominant states, respectively. In contrast to many other black hole spectra, high energy complexity in the form of a break or cut-off is not required for the hard state, contrary to previous expectations for this state. We show for the first time that Comptonization by non-thermal electrons is the dominant process for the high energy emission in the hard state. We discuss our results in terms of models for broad-band emission and accretion flows in stellar-mass black holes.

¹LAEFF-INTA, P.O. Box 50727, 28080 Madrid, Spain, mcaballe@laeff.inta.es

²Department of Astronomy, University of Michigan, 500 Church Street, Ann Arbor, USA, MI 48109, jonmm@umich.edu

³ESA/ESAC, Urb. Villafranca del Castillo, PO Box 50727, 28080 Madrid, Spain

⁴MIT Kavli Institute for Astrophysics and Space Research, 77 Massachusetts Avenue, Cambridge, MA 02139, USA

⁵CAB (CSIC-INTA) P.O. Box 50727, 28080 Madrid, Spain

⁶Astronomical Institute “Anton Pannekoek”, Kruislaan 403, University of Amsterdam, Amsterdam, 1098 SJ, The Netherlands

⁷University of Cambridge, Institute of Astronomy, Cambridge CB3 0HA, UK

⁸School of Physics and Astronomy, University of Southampton, Highfield, Southampton, SO17 1BJ, UK

Subject headings: Black hole physics – stars: binaries (GRO J1655–40) – gamma rays: observations – accretion, accretion disks – radiation mechanisms: non-thermal – radiation mechanisms: thermal

1. Introduction

GRO J1655–40 is a black hole X-ray binary whose parameters are well known. Also called Nova Scorpii 1994, the source was discovered with the Burst and Transient Source Experiment (BATSE) on board the Compton Gamma-Ray Observatory (CGRO) on 1994 July 27 (Zhang et al. 1994). The optical counterpart was discovered soon after by Bailyn et al. (1995) ($V \sim 14.4$ mag). Subsequent optical studies regarding the properties of the light curve during the outburst and quiescent period showed that the system is an LMXB composed of a blue subgiant (spectral type F4 IV) as the secondary and a black hole (hereafter BH) as the primary ($m_{\text{BH}} = 7.02 \pm 0.22 M_{\odot}$, Orosz & Bailyn (1997)). The system is located at a distance of 3.2 kpc as measured by Tingay et al. (1995). Although Foellmi et al. (2006) have recently suggested a smaller distance, their parameters imply that the donor star would not fill its Roche lobe. Bailyn et al. (1995b) established the orbital inclination of the system to be $\simeq 70^\circ$ (see also Orosz et al. (1997) and van der Hooft et al. (1998)); an independent determination made by Kuulkers et al. (1998) based on X-ray flux dips constrained the inclination of the system to be $60^\circ - 75^\circ$. The inclination of the inner disk may be as high as 85° , indicating a slight mis-alignment with the binary system (Hjellming & Rupen 1995).

GRO J1655–40 has displayed some of the most extreme behavior and phenomena yet observed from any black hole X-ray transient. Strohmayer (2001) discovered a pair of high-frequency quasi-periodic oscillations (QPOs) at 300 and 450 Hz in power spectra from the 1996/1997 outburst of the source. If the higher frequency is associated with the Keplerian frequency at the innermost stable circular orbit (ISCO, Shapiro & Teukolsky (1983), located at $R_{\text{ISCO}} = 6 R_g$ for a Schwarzschild black hole or at $R_{\text{ISCO}} = 1.25 R_g$ in the case of a maximal Kerr BH of $a = 0.998$; where $R_g = GM/c^2$ is the gravitational radius and $a = cJ/GM^2$; see Bardeen et al. (1972) and Thorne (1974)), the frequency observed indicates that GRO J1655–40 harbors a spinning black hole. This suggestion is broadly consistent with spin estimates based on fits to skewed Fe K emission lines ($a \geq 0.9$ as per $r \leq 1.4 R_g$, Miller et al. (2005)). GRO J1655–40 has also ejected extremely relativistic radio jets (Hjellming & Rupen 1995). Finally, unbroken power-law emission (i.e. without a cutoff) from GRO J1655–40 has been detected out to 800 keV (Tomsick et al. 1999), offering a crucial insight on high energy processes in black hole systems.

High energy processes and the periods of correlated behavior known as “states” in black hole binaries are the focus of this paper. Three active states are commonly recognized in the soft X-ray domain (see Remillard & McClintock (2006)): the non-thermal dominant or hard state (formerly called low/hard), the thermal-dominant state (formerly called high/soft), the steep power law state (hereafter SPL). Additionally there are transitions between these states which are often referred to as intermediate states. In the hard state, the soft X-ray emission is very weak and the spectrum is dominated by some kind of non-thermal emission that is broadly consistent with a power law (hereafter PL) at higher energies ($\gtrsim 20$ keV). It has been known for a long time that black hole spectra in the hard state are exponentially cut off at ~ 100 keV (see Grove et al. (1998) and references therein). A radio jet is usually inferred in this state from flat radio spectra (see Fender et al. (2004) for an unified model for X-ray states and radio emission in black hole X-ray transients). In the thermal-dominant state, the disk dominates the X-ray emission. Although high energy emission ($\gtrsim 20$ keV) also is seen in this state, it is weaker, generally steeper, and extends up to 800 keV without any break (Grove et al. 1998). In the SPL, these emission components are combined – both the disk and the non-thermal power-law are strong, although the disk no longer follows the $L \propto T^4$ relation that is observed in the soft state (Kubota et al. 2001); (Saito et al. 2007).

Several models have been proposed to explain the physical conditions of the innermost accretion flow and the nature of hard X-ray emission in the various states, but a clear picture has not yet been achieved. At low mass accretion rates hard X-ray emission may arise in an inner region filled by a hot ($kT_e \sim 100$ keV), radiatively inefficient, advection-dominated accretion flow (ADAF) (Narayan (1996), Esin et al. (2001)). A recent study made by Yuan & Zdziarski (2004) shows that the ADAF scenario is not able to explain the relatively high luminosities that have been observed in the hard state of some black-hole X-ray binaries. Alternatively, some recent models suggest that direct synchrotron emission, and/or synchrotron self-Comptonization in a jet may dominate the hard X-ray emission (Markoff et al. (2001), Markoff et al. (2003), Markoff et al. (2005)). Both at low and high mass accretion rates thermal Comptonization in a corona (fed by seed photons from the disk) may also be an important source of hard X-ray emission (see, e.g., Frontera et al. (2003)). An alternative source of Comptonization which is less reliant on the disk is bulk motion Comptonizing (BMC, Ebisawa et al. (1996); see also Titarchuk & Shrader (2002) for a co-moving Comptonizing medium). In this case, the Comptonization is due to bulk motion of an almost free falling (convergent accretion) flow close to the black hole.

A thermal distribution of the Comptonizing particles (electrons) necessarily leads to a turnover in the emitted spectrum around kT ; therefore, thermal Comptonization should lead to a turnover near to the electron temperature of the corona, kT_e . Synchrotron emission and non-thermal electron distribution do not necessarily predict such a turn-over, however, and

this difference provides an observational tool to distinguish which processes dominate the hard X-ray emission in different black hole states. The high energy sensitivity of INTEGRAL is especially well-suited to this purpose.

In this paper, we report on observations of GRO J1655–40 made with INTEGRAL during the outburst which began in February of 2005 (Markwardt & Swank 2005). In Section 2 we describe our observations and in Section 3 we show the light curves obtained with JEM-X, ISGRI, SPI and OMC (instruments on-board INTEGRAL) and RXTE and discuss the possible origin of their evolution. In Section 4 we present our spectral analysis made with JEM-X, ISGRI and SPI. Finally, in Section 5 we discuss our results in the context of the different models and theories present in the literature.

2. Observations

2.1. INTEGRAL observations

The data were obtained with INTEGRAL and cover the first part of the 2005 outburst using the following instruments: the SPectrometer on INTEGRAL (SPI; Vedrenne et al. (2003)), the INTEGRAL Soft Gamma-Ray Imager (ISGRI; Lebrun et al. (2003)), the Joint European X-ray Monitor (JEM-X; Lund et al. (2003) and the Optical Monitoring Camera (OMC; Mas-Hesse et al. (2003)). ISGRI is optimized for 15 keV to 10 MeV imaging and SPI is optimized for high-resolution spectroscopy in the 18 keV to 8 MeV band. The former provides an angular resolution of $12'$ full-width half maximum (FWHM) and an energy resolution, $E/\Delta E$ of ≈ 12 (FWHM) at 100 keV. SPI provides an angular resolution of 2.8° (FWHM) and an $E/\Delta E$ of 430 FWHM at 1.3 MeV. JEM-X has a fully coded Field of View (FOV) of 4.8° diameter and an angular resolution of $3'$ FWHM. JEM-X has medium resolution spectral capabilities in the energy range of 3–35 keV. The OMC is an optical monitor, with a FOV of $5^\circ \times 5^\circ$ and an astrometric resolution of < 1 arcsec, and performs optical photometry in the V-band down to 18^{th} magnitude.

Our program consisted of 4 ToO observations of 100 ks each, spread from 27 February to 11 April of 2005 (we will refer to these as epochs 1–4 below; see Table 1 for more details). The difference in the exposure times between the INTEGRAL instruments given in Table 1 (JEM-X, ISGRI and SPI) are due to the difference in the dead times and variation in the efficiency along the fields of view. The dithering pattern used during the observations was 5×5 (square of 25 pointings separated by 2.17 degrees centered on the main target of the observation); this is the best pattern in order to minimize background effects for the SPI and ISGRI instruments in crowded fields. Data reduction (in the case of JEM-X, ISGRI and

SPI) was performed using the standard Off-line Science Analysis (OSA) 5.1 software package available from the INTEGRAL Science Data Centre (ISDC; Courvoisier et al. (2003)). In the case of SPI, because of the lower angular resolution and crowded field of view in γ -rays at this position of the sky $(l,b)=(344.98^\circ,+2.46^\circ)$, (see Figure 1), we used a non-standard procedure in the analysis of the data, described in Deluit (2005) and Roques & Jourdain (2005). For the same reason, in the case of OMC, we used a standard pipeline available in OSA 6.0 (recently delivered) for extraction of fluxes. For OMC all the public data available from ISDC were downloaded (this resulted only in a slight increase in the ammount of data). Because of the steep fall in response in the case of JEM-X, and because of its reduced FOV ($\approx 5^\circ$ of diameter), we limited the pointing radius with respect to the GRO J1655–40 position to be within 4° . In the case of SPI and ISGRI, with large Fully Coded Fields of Views (FCFOV) ($16^\circ \times 16^\circ$ for SPI and $8.3^\circ \times 8^\circ$ for ISGRI), pointing selections were not necessary. In total, 199 individual pointing (or Science Window – each having exposure times lasting from 1800 to 3600 s and following a 5×5 dithering pattern on the plane of the sky Courvoisier et al. (2003)) data were used for both SPI and ISGRI, 96 pointings for JEM-X and 66 pointings for OMC.

2.1.1. *Extraction of light curves*

GRO J1655–40 was covered with INTEGRAL as part of the Galactic Bulge Monitoring Program (Kuulkers et al. 2007). Precisely at the start of this program GRO J1655–40 was reported to become active (Markwardt & Swank 2005). The subsequent outburst of GRO J1655–40 was also followed with the RXTE/ASM and with a dense program of pointed RXTE/PCA observations (Homan 2005). In Figure 2 we show the ISGRI (20–60 and 60–150 keV), RXTE/ASM (2–12 keV) and OMC (optical) light curves. The light curve derived from the IBIS/ISGRI in the 20–60 and 60–150 keV energy bands had 1800 sec exposures (about 150 counts/s correspond to 1 Crab on-axis in the 20–60 keV energy band, see Appedix A in Kuulkers et al. (2007)). GRO J1655–40 was observed at a large off-axis angle ($\approx 15^\circ$ from the center of the field of view; so is in the partially coded field of view of IBIS/ISGRI and not visible with X-ray monitor JEM-X).

Since GRO J1655–40 is located in a very crowded FOV for the OMC, in the flux extraction process we force the photometric aperture to be centered at the source coordinates, which are taken from the OMC Input Catalogue (Domingo et al. 2003).

The typical limiting magnitude of the OMC in the Galactic bulge is between $V = 15$ and $V = 16$ (3σ). This value depends strongly on sky background and source contamination. In our case $(l,b)=(344.98^\circ,+2.46^\circ)$ we can confidently get limiting magnitudes down to $V = 16$

(3σ). For each INTEGRAL pointing, the OMC monitors the sources in its FOV by means of shots of variable integration time. Typical values in the range 10 to 200 s (currently 10, 50 200 s) are used to optimize sensitivity and to minimize read-out noise and cosmic-ray effects. For the faintest objects, several 200 s exposures in the same pointing can be combined during data analysis on the ground. We obtained one photometric point by combining several 200 s OMC shots. To increase the signal to noise ratio, we combined the individual photometric points of every pointing and calculated the final photometric points by making running averages in order to minimize the dispersion.

2.1.2. Extraction of spectra

For JEM-X and ISGRI, individual spectra were obtained for each pointing. The spectra were then combined to obtain an averaged spectrum per epoch using the *spe_pick* OSA tool and standard procedures (see Chernyakova (2005) and Chernyakova et al. (2005)) to rebin the response matrices. In the case of SPI, we derived directly one spectrum per revolution. The SPI spectra were extracted over an energy range of (23-800) keV (with 26 logarithmic bins) using the SPIROS package within OSA, applying maximum likelihood optimization statistics (Skinner & Connell 2003). Due to the crowdedness of the field and the low spatial resolution of the instrument (i.e. sources separated less than 2.8° can not be resolved) it was necessary to apply special techniques to extract spectra (see Roques & Jourdain (2005) and Deluit (2005)). This included accounting for variability of the sources present in the FOV. The background ¹ was determined by using flat fields from particular INTEGRAL revolutions (revolution 220 in our case – i.e. the time closest publicly available flat field to our period of observations), and the use of background method 3 (determination of the background based on some specific flat field INTEGRAL observations). Due to the fact that SPI is a high resolution spectrograph in its energy range (20-8 000 keV) with a reduced number of detectors (namely, 19) it is not optimized in the detection of sources without taking into account previous information about the spatial distribution of them. Thus, we used as an input catalog of sources those obtained from the ISGRI in the (20-40) keV mosaic images (see Figure 1).

¹Due to the fact that JEM-X, ISGRI and SPI are detectors based in coded mask optics, the detection of sources is made in basis of a deconvolution process, taking also into account background, in an iterative process called IROS (Iterative Removal Of Sources). In OSA 5.1 the spectra obtained are always background subtracted and it is not necessary to apply in XSPEC any background correction to the obtained spectra. The light curves obtained are also background subtracted. However, in JEM-X analysis it is possible to skip the level of background subtraction. We refer to the Roques et al. (2005b), Goldwurm et al. (2003), Westergaard et al. (2003) and Dubath et al. (2005) for more details.

The signal from GRO J1655–40 was too soft to detect any emission in the last two epochs with SPI. We combined single revolution SPI spectra from each epoch, since there was no significant evolution and in order to increase the signal to noise ratio. This resulted in one SPI spectrum in revolution 290 and another one combining the revolutions 295 and 296. The same was done for the low energy instruments (JEM-X and ISGRI), thus obtaining four spectra, namely one for each epoch, as can be seen in Table 1. We applied 2% systematic errors to the JEM-X, ISGRI and SPI spectra. We restricted our analysis in the energy ranges of 5 – 30, 23 – 600 and 23 – 800 keV for the JEM-X, ISGRI and SPI spectral analysis, as recommended in Lubiński et al. (2005). The SPI and ISGRI spectra were rebinned at high energies ($\gtrsim 200$ keV) with the FTOOL *grppha* procedure to reach the detection level of 3σ .

3. Analysis of light curves

Figure 2 shows the GRO J1655–40 light curves obtained with ISGRI (from the INTEGRAL Galactic Bulge Monitoring Program; Kuulkers et al. (2007)) in two energy bands (60-150 keV and 20-60 keV) together with the OMC (optical). The public RXTE/ASM (2-12 keV) light curve in the same period of time is shown in the same Figure for comparison.

The light curve in Figure 2 does only show the first month of outburst of GRO J1655–40. For a full outburst light curve, refer to Brocksopp et al. (2006). Brocksopp et al. (2006) show the X-ray light curve obtained by SWIFT, jointly with that obtained in the optical and ultraviolet band using the Ultraviolet/Optical telescope on-board SWIFT (UVOT). In Figure 3 we show the RXTE/PCA light curve in the range (2-60) keV plus a hardness ratio (calculated as the ratio of the 9.4-18.2 keV and 2.8-5.7 keV count rates) evolution of the source during the entire outburst, taken from Homan et al. (2007). The light curves were made from 520 RXTE observations, with one (averaged) data point for each observation. The horizontal lines shown in Figures 2 and 3 indicate the time intervals (100 ks each; in 4 observations) over which our average spectra were obtained. Note that black hole transients usually begin and end their outbursts in the hard state (see Nowak (1995), Fender et al. (2004), Homan & Belloni (2005)) and the 2005 outburst of GRO J1655–40 is no exception. As can be seen in Figure 2, the beginning of the outburst first started at high energies (20 – 150 keV) rather than at softer X-rays (2 – 10 keV). Moreover, as can also be seen from the hardness ratios in Figure 3, the observations of epoch 1 correspond to the hard state of black holes (see Section 5). The other three epochs were done during a period when the source spectrum was much softer. However, it should be noted that it was only later in the outburst that the softest spectra (corresponding to the thermal-dominant state) were observed (see Figure 3).

The first indications of an impending outburst of GRO J1655-40 came from RXTE/PCA bulge-scan observations on 2005 February 19 (Markwardt & Swank 2005). On February 20, observations made with the PANIC camera on the 6.5 m Magellan-Baade telescope at Las Campanas Observatory revealed a J-band (near-infrared) magnitude of $J=13.2\pm0.1$ (Torres et al. 2005), indicating that GRO J1655-40 was brighter by ≈ 0.5 mag in J relative to its magnitude in quiescence ($J=13.7-14$) (Greene et al. 2001). On the same date a radio detection of the source was reported (Rupen et al. 2005).

As can be seen from Buxton & Bailyn (2005) and Brocksopp et al. (2006) the optical light curve behaves differently from the X-rays. The optical behaviour consists of an increase in the flux until a constant level at MJD=53 455. This behaviour can also be seen with the OMC, because the flux in the optical light curve was increasing, reaching a constant and detectable value ($V\sim 15$ mag) in MJD=53 455. Then the optical flux became constant. It is also interesting to note the rapid increase of the radio emission at MJD \approx 53 450, coinciding with our epoch 3 of observations and also with the beginning of the plateau in both the optical and infrared light curve.

4. Spectral analysis of INTEGRAL data

We performed fits to the combined JEM-X, ISGRI and SPI spectra, for each of the four epochs (see Table 1) using XSPEC (Arnaud 1996) v.11.3. All errors quoted in this work are 90% confidence errors, obtained by allowing all variable parameters to float during the error scan. In all fits, we fixed the value of the column density to $N_H = 8.0 \times 10^{21}$ atoms/cm² as obtained by Díaz Trigo et al. (2006) using XMM-Newton data of GRO J1655-40 during the same outburst.

Our main aim in these fits is to characterize the broad continuum as seen with INTEGRAL and its broad energy coverage. To account for uncertainties in relative instrument calibrations, we fixed JEM-X multiplicative calibration constant to 1 and let that of ISGRI and SPI free to vary in the fit for the different data sets as shown in Table 2.

In Figures 6, 7, 8, 9 and 10 we show spectra from each epoch because these provide a convenient way to see the evolution of the source during our observations. We fitted the spectra with several models and the derived parameters are presented in Table 2. We modelled the spectra with simple and phenomenological disk plus power-law models and common Comptonization models described in Section 1. We find that the former are very successful (see Section 4.1.1), and there is no evidence for any spectral break in the data up to ≈ 600 keV (see Section 4.1.2). Although a simple power-law provided marginally acceptable

fits in the first two epochs, it was necessary to include an iron line and edges components in the fits of the last two epochs (see Section 4.2).

4.1. Fits of the former two epochs

4.1.1. Fits with a pure power-law

We initially performed fits with a phenomenological power-law model (*powerlaw* model in XSPEC) in the spectra that extend up to 600 keV.

In the first epoch, the source spectra extend in the energy range of 5 – 20 keV for JEM-X and 23 – 600 keV for both ISGRI and SPI, respectively. In fitting with the *power-law* model, we obtained a reduced chi-square of $\chi^2_\nu = 1.26$ with $\nu = 63$ (ν meaning the number of the degrees of freedom of our fit). The presence of a multicolor disk component was not significantly required in our fit. The value obtained for the photon index was $\Gamma = 1.72 \pm 0.03$, common for black holes in a hard spectral state.

For the second epoch of our observations, the source spectra extend in the energy range of 5 – 30 keV, 23 – 500 keV and 23 – 400 keV for JEM-X, ISGRI and SPI, respectively. This time the presence of emission coming from a disk was significant, and we added an absorbed multicolor disk component (Mitsuda et al. 1984) to the power-law (*phabs(diskbb+powerlaw)* model in XSPEC). We obtained $\chi^2_\nu = 1.38$ with $\nu = 88$. The value obtained for the inner disk temperature was $kT_{in} = 1.25 \pm 0.01$ keV. The spectrum is softer, with a value for the photon index of $\Gamma = 2.21 \pm 0.04$.

For the last two epochs, in fitting with a phenomenological power-law (plus a multicolor disk black body component), the spectra showed large negative residuals at ≈ 10 keV, compatible with the presence of *Fe* edges. The presence of positive residuals in the range 6 – 8 keV is consistent with the presence of a broad *Fe* emission line. In Section 4.2 we go into more detail on the fits of both these epochs.

4.1.2. Fits with thermal Comptonization models

As explained in Section 1, all models involving thermal Comptonization processes as the origin of the high energy emission seen in black hole transient systems predict an energy turn-over at the electron temperature of the corona. So, in order to assess the role of Comptonization during the time of our observations, we fitted with the thermal Comptonizing model of Titarchuk (1994) (called *CompTT* in XSPEC), which deals with the special

case of high temperatures and/or small opacities (so the relativistic effects are taken into account). We also made fits using the BMC model of Ebisawa et al. (1996) (see also Titarchuk & Shrader (2002) for a co-moving Comptonizing medium), which deals with the Comptonization due to bulk motion of the almost free falling (convergent accretion) flow close to the black hole. Moreover, we fitted with a phenomenological and multiplicative cutoff (called *highcut* in XSPEC) model in order to find any turn-over energy in our data which could be in agreement with Comptonization models playing the major role in the high energy emission of GRO J1655–40.

We thus fitted the spectra of the first two epochs² with following models: *phabs(diskbb+powerlaw)highcut* (hereafter called model 1), and *phabs(diskbb+compTT)* (hereafter called model 2) and *phabs(bmc)highcut* (hereafter called model 3). In the case of the first epoch, the presence of a multicolor disk component was not significantly required in our fit. We assumed a spherical geometry for the Comptonizing medium for the model 2 in all our fits.

For epoch 1 of our observations, we obtained the following statistics for all three models, i.e. $\chi^2_\nu = 1.13, 1.17, 1.13$ ($\nu = 61, 60, 59$), respectively. We find that when fitting the data with a cut-off power-law (model 1), while showing slightly better statistics, the high energy cut-off can not be well constrained (values between 5 and 54 keV are compatible with the data). The obtained folding energy is > 253 keV. We made fits to separate JEM-X+ISGRI and JEM-X+SPI to see if in one of the two data sets a break is possible. In the former, we obtained unconstrained values for the cut-off and the folding energies, being in the ranges of 5–38 keV and > 238 keV, respectively. In the second data set there was not any break in the data as well. We conclude that the cut-off features found are of instrumental origin and are not physically meaningful. Thus, there is not any real cut-off in our data. This issue is also supported by the fact that the parameters optical depth and temperature of the electrons (τ and kT_e) when fitting with model 2 are unconstrained as well. This model clearly is not a good description of the high energy spectrum ($\gtrsim 20$ keV). The model 3, while giving the lowest residuals, does not allow to constrain the values for the parameters (neither of *bmc* and *highcut* components). Thus, this model does not represent a physical description of the data. The fact that model 3 provides slightly better statistics than the power-law model described in Section 4.1.1 would be due to the fact that this model is a convolution of both soft and hard emission components taking into account the physical condition in the inner region of the accretion disk. We derive from fitting with all these models that high energies

²As we explained in Section 4.1.1 the presence of significant residuals compatible with broad *Fe* emission line, edges and likely reflection could distort our understanding of the continuum. Thus, we do not use last two epochs in our study of the continuum models. Moreover, the spectra in these epochs do not show significant emission at high ($\gtrsim 150$ keV) energies.

can not be reproduced by thermally upscattering photons by a Comptonizing corona alone. In order to take this issue into account, we fitted the spectrum of this epoch with the hybrid Comptonization model EQPAIR (Coppi 1999) proper for very hot plasmas which describes the physics and emission properties of hybrid plasmas, where the particle distribution energy is approximately a Maxwellian plus a power-law. This model deals a hot plasma cloud, mainly modeled as a spherical corona around the compact object, illuminated by soft thermal (Maxwellian) and non-thermal (either power-law or monoenergetic distributed) electrons that lose energy by Compton, Coulomb and bremsstrahlung interactions. This model was shown to be successful in accounting for the high energy spectra of Cygnus X-1 and other black hole candidates in different spectral states and over a broad energy band ranging from soft X-rays to gamma-rays (see e.g. McConnell et al. (2000), McConnell et al. (2002), Cadolle et al. (2006), Malzac et al (2006)).

For epoch 2 of our observations, we obtained the following statistics for all three models, i.e. $\chi^2_\nu = 1.47, 1.45, 2.07$ ($\nu = 86, 87, 86$), respectively. Again, model 1 does not show a break or cut-off below 500 keV (i.e. values of both cut-off and folding energies can not be constrained) and model 3 is not a proper fit to the data due to the bad statistics. In this epoch, the values obtained for the optical depth of the Comptonizing medium and the temperature of the electrons (τ and kT_e) can not be constrained. Thus, the data show that thermal Comptonization is not the main process that generates the emission at high energies ($\gtrsim 20$ keV). As in epoch 1, we tested the model of Coppi (1999), optimized for very hot coronae (see description in paragraph above), this time coupled with *diskbb* component to describe the soft emission from the accretion disk.

4.1.3. Fits with the EQPAIR non-thermal Comptonization model

This model (EQPAIR) takes into account angle dependence, Compton scattering (up to multiple orders), photon pair production, pair annihilation, bremsstrahlung as well as reflection from a cold disk. As noticed by Coppi (1999), if a spectrum extends up to 500 keV high energy emission coming from a non-thermal population of electrons is clearly present.

As can be seen in Figure 4 and 5, in which we fitted both 1 and 2 epochs with a single power-law (see description in Section 4.1.1), an small deficit of counts of the ISGRI spectra above 200 keV with respect to SPI is clearly present. Moreover, the large bins of ISGRI spectra in this range of the spectra, would indicate that the source is not detected above 200 keV. This is a comprehensive issue since SPI instrument is optimized for doing spectroscopy up to 1 MeV while ISGRI has poorer sensitivity above 200 keV. Taking these

considerations into account, we limited our analysis of ISGRI data in the energy range of 23 – 200 keV.

The *eqpair* model allows to inject a non-thermal electron distribution with Lorentz factors between γ_{min} and γ_{max} and a power-law spectral index Γ_p . The cloud is illuminated by soft thermal photons emitted by an accretion disk. These photons serve as seed for Compton scattering by both thermal and non-thermal electrons. The systems is characterized by the power (i.e. luminosity) L_i supplied by its different components. We express each of them dimensionlessly as a compactness parameter, $l_i = L_i \sigma_T / (R m_e c^3)$, where R is the characteristic dimension and σ_T the Thompson cross-section of the plasma. Thus, l_s , l_{th} , l_{nth} and $l_h = l_{th} + l_{nth}$ correspond to the power in soft disk entering the plasma, thermal electron heating, electron acceleration and the total power supplied to the plasma. The total number of electrons (not including e^+ and e_- pairs) is determined by τ , the corresponding Thompson optical depth, measured from the center to the surface of the scattering region. We considered the source to be moderately compact and fixed $l_s = 10$, as broadly reported for other sources with similar characteristics.

The disk spectrum incident on the plasma is modelled with a multicolor disk blackbody as given by the *diskbb* model in XSPEC of Mitsuda et al. (1984). The temperature of the inner edge of the accretion disk was fixed to $kT_e = 0.5$ keV. The limits of the accretion disk were fixed to $R_{max} = 100R_g$ and $R_{min} = 6R_g$. We attempted to fit both spectra of epochs 1 and 2 fixing the reflection covering factor to zero.

For epoch 1 of our observations we first performed a fit with non-thermal electrons injected with a power-law distribution of Lorentz factors from $\gamma_{min} = 1.3$ to $\gamma_{max} = 1000$. The upper and the lower limits γ_{min} and γ_{max} were kept fixed while fitting the power-law index Γ_p . This resulted in an acceptable fit with a reduced chi-square of $\chi_\nu = 1.21$ ($\nu = 57$). The unfolded broadband spectrum and residuals are shown in Figure 6. The best fit paramaters are presented in Table 2. l_h/l_s is about unity, i.e. intermediate between what is found in the hard state (4-10) and the thermal dominant state (≤ 0.4) (Ibragimov et al. 2005). The heating of the plasma is dominated by the non-thermal acceleration ($l_{nth}/l_h \approx 1$). We also fitted the spectra of this epoch considering a mono-energetically distributed population of non-thermal injected electrons instead. The obtained reduced chi-square is slightly better ($\chi_\nu = 1.19$, $\nu = 57$). The values obtained for l_h/l_s and l_{nth}/l_h remained unchanged, except for an increasing of the Thompson scattering depth (from 1.0 ± 0.6 to 2.7 ± 0.4 , for the former and the second fit, respectively). The increasing of the optical depth gives support to the scenario of Comptonization through injected non-thermal electrons as being the dominant mechanism in the sense that if this is done by electrons with a mono-energetic distribution then a denser cloud would produce the same effect as taking into account a broader distribution (both

in energy and spatially). Thus, we conclude that in order to reproduce the spectrum of first epoch, we have to consider an almost purely distribution of non-thermal accelerating particles.

As in epoch 1, we tested the model of Coppi (1999), optimized for very hot coronae in observations of epoch 2, this time coupled with *diskbb* component to describe the soft emission from the accretion disk. We performed a fit with non-thermal electrons injected with a power-law distribution of Lorentz factors from $\gamma_{min} = 1.3$ to $\gamma_{max} = 1000$. The upper and the lower limits γ_{min} and γ_{max} were kept fixed while fitting the power-law index Γ_p . This resulted in an acceptable fit with a reduced chi-square of $\chi_\nu = 1.44$ ($\nu = 83$). The unfolded broadband spectrum and residuals are shown in Figure 7. The best fit parameters are presented in Table 2. l_h/l_s again is about unity. However, the heating of the plasma by non-thermal particles is practically zero ($l_{nth}/l_h \approx 0$). The situation does not improve by considering a mono-energetic distribution of the non-thermal accelerated electrons. This issue is not surprising, since, as claimed by Coppi (1999), a very good spectrum extending above 200 keV is mandatory in order to disentangle a likely population of non-thermal particles in the source. In the case of our observations, the large bin at ≈ 200 keV shows that the source was not detected above this energies. We conclude that while in epoch 2 of our observations a break is not observable in the high energy data $\gtrsim 20$ the energy coverage is not great enough in order to test the presence of non-thermal processes. This is due to the fact that in this period the spectrum became to be very soft, compared to epoch 1, with radiation detected to ≈ 200 keV as maximum.

4.2. Fits to epochs 3 and 4

4.3. Fits with *Fe* emission line and absorption edges

As shown in the shape of the residuals (see Figure 8), fits with simple multicolor disk model of Mitsuda et al. (1984) and power-law did not give formally acceptable fits to the last two epochs. The presence of large residuals at 6 – 8 keV and around 10 keV require us to take into account iron emission line, iron absorption edges and likely disk reflection components. These features are theoretically required in very ionized mediums as the close vicinity of the black holes (see Ueda et al. (1998) for a former detection of *Fe* absorption lines and edges in GRO J1655–40 in the context of observations of the 1996 outburst and George & Fabian (1991) and Laor (1991) for a description of the *Fe* line profile produced in accretion disks around black holes). The reflection component takes into account the physical condition of the Compton-reflected continuum of a source of hard X-rays by an accretion disk (Gilfanov et al. 2000).

We fitted our spectra with the following model: *phabs(diskbb+powerlaw+gaussian)edge** *edge* and the results of the fits are shown in Table 2. Regarding the Gaussian *Fe* emission line component, we constrained the line center in the range of 6.4 – 6.97 keV, which is the allowed range due to the different ionization states of *Fe*. Also, we constrained the width (σ) of the iron emission line to be 1 keV as a fiducial maximum value in order to get convergence of our fits. Regarding the two iron absorption edges, one was fixed at 9.278 keV, which corresponds to Fe XXVI and is expected to appear given the likely range of temperatures and ionization.

Fitting this model to the spectra for epochs 3 and 4, we obtained better results than fitting with a power-law model (plus an absorbed multicolor disk), i.e. $\chi^2_\nu = 9.99$, with $\nu = 21$, and $\chi^2_\nu = 2.73$, with $\nu = 22$, for the third and fourth epoch, respectively. Although the fit was unacceptable for the third epoch, because of the large residuals at around $\approx 10 - 20$ keV, which could be due to reflection ³, the fit was reasonable for fourth epoch. The multicolor disk component gave an inner disk temperatures of $kT_{in} = 1.27 \pm 0.17$ keV for the fourth epoch, in which we also obtained a very soft photon index ($\Gamma = 4.7 \pm 0.6$).

We substituted the *power – law* component by the *pexriv* reflection model in the third epoch. This component is a power-law with an exponential cut-off in order to take into account reflection effects in the spectrum. In fitting with the *pexriv* model, we imposed an overabundance of *Fe* of 2.8 with respect to the solar value and $\cos(i) = 0.45$, the last implying an inclination of 63° for the inclination of the reflection medium, namely the disk (as found by Díaz Trigo et al. (2006) based on XMM and INTEGRAL data for the same period of observations). The temperature of the disk that gave the smallest residuals was $T_{disk} = 1.2 \times 10^{+07}$ K so we fixed this value in our fits. This value is consistent with having very ionized material in the accretion disk. Also, in order to properly fit the high energy part of the spectra ($\gtrsim 20$ keV) it was necessary to fix the *pexriv* e-folding energy to a very high value, namely 1000 keV, implying a non-detection of any cut-off up to ≈ 200 keV.

As a result of this fit for third epoch, we obtained a reflection covering factor of $R \leq 0.3$. Actually, this value (R) approximately measures the solid angle subtended by the reflecting medium as seen from the source of the primary radiation, $R \approx \Omega_{refl}/2\pi$, so that $R = 1$ for an isotropic point source above an infinite optically thick slab. We fixed the ionization parameter to a very high value, consistent with a very high ionization medium, $x_i = 4\pi F_{ion}/n = 5000$ erg \times cm/s (where F_{ion} is the 5-20 keV irradiating flux and n is the

³It is important to notice that Díaz Trigo et al. (2006) did not find reflection signatures in the analysis of joint XMM and INTEGRAL data corresponding to our fourth epoch. The disagreement could be due to the 20 – 30 keV removed bin in their study, made in order to improve the statistics for the joint spectrum obtained in this period.

density of the reflector; see Done & Nayakshin (2001)).

In order to estimate the source luminosity in each of our observations, we used the power-law plus an absorbed multicolor disk model for all the epochs. The contribution of the iron emission and absorption effects together contribute only by $< 10\%$ of our data in the last two epochs. The un-absorbed flux in the range of 5 – 100 keV energy range is $F(5 - 100)_X = 1.4 \times 10^{-9}, 1.2 \times 10^{-8}, 1.0 \times 10^{-8}, 1.0 \times 10^{-8}$ erg cm $^{-2}$ s $^{-1}$ for the first to fourth epoch, respectively. For a distance of 3.2 kpc (Tingay et al. 1995), these fluxes give luminosities in the (5 – 100) keV energy range of $L(5 - 100)_X = 1.7 \times 10^{36}, 1.5 \times 10^{37}, 1.2 \times 10^{37}, 1.2 \times 10^{37}$ erg/s. The un-absorbed fluxes in the 5-600 keV energy range are $F(5 - 500)_X = 3.7 \times 10^{-9}, 1.2 \times 10^{-8}, 1.0 \times 10^{-8}, 1.0 \times 10^{-8}$ erg s $^{-1}$ cm $^{-2}$, giving luminosities of $L(5 - 600)_X = 4.6 \times 10^{36}, 1.5 \times 10^{37}, 1.2 \times 10^{37}, 1.2 \times 10^{37}$ erg/s for the first to fourth epochs, respectively. Even if we take the broader energy range as more indicative of the true source luminosity, these values represent only 0.5%, 1.5%, 1.3%, and 1.3% of the Eddington limit ($L_{\text{EDD}} = 9.4 \times 10^{38}$ erg/s for a black hole of $7 M_{\odot}$), respectively.

5. Discussion and Conclusions

We have made fits to four epochs of INTEGRAL broad-band spectra of the stellar-mass black hole GRO J1655–40 during its 2005 outburst. We find that GRO J1655–40 was in the hard state in the first epoch, based on the low photon index (i.e. 1.72 ± 0.03) and the absence of a strong thermal disk component. The source evolved to a state that resembles a thermal dominant state in the classification scheme of Remillard & McClintock (2006). These statements are in agreement with the previous study of this outburst by Brocksopp et al. (2006). However, Saito et al. (2007), on the basis of their analysis of RXTE/PCA data of this source, showed that the luminosity of the accretion disk deviates from the $L \propto T^4$ relation typical of thermal-dominant states during our other 3 observations (epochs 2, 3 and 4). So, the state observed may not be a true thermal-dominant state, and/or non-thermal effects may need to be modeled to describe the accretion disk emission (Kubota et al. 2001).

For the two latest epochs, we found that our data is best fitted by adding an iron emission line and edges in the model consisting of an absorbed multicolor disk (Mitsuda et al. 1984) plus a power-law component. Although the obtained fits were not formally acceptable ($\chi^2_{\text{red}} = 9.99, 2.73$ for the third to fourth epochs, respectively), the fit in the fourth epoch was improved by $\Delta\chi^2_{\text{red}} = 4.8$. Also, the shape of the residuals using the model consisting of a multicolor disk black body plus a power-law showed a clear excess in the 6 – 8 keV range and a drop at around 10 keV, features that can only be explained by the presence of iron emission line and the presence of *Fe* edges. The spectrum in the third epoch showed an

excess of absorption in the 10 – 20 keV energy range with respect of that expected taking into account the edges obtained in Díaz Trigo et al. (2006) based on XMM and INTEGRAL spectra (see Section 4.2). This excess could be explained by the presence of reflection, but the situation is still unclear. We attempted to deal with this feature in third epoch by fitting with a broken power-law model (*pexriv* in XSPEC) but there is no clear evidence for a break in this spectrum. We conclude that for GRO J1655–40, it is difficult to study reflection features. This may be due to the high inclination of the source, which could alter the shape of the reflection features through scattering. The presence of these features in the spectra of epochs 3 and 4 may reveal differences in the disk outflow properties with respect to any outflow in epochs 1 and 2. In fact, our spectrum obtained in epoch 3 precedes a *Chandra* observation revealing a line-rich spectrum (Miller et al 2006) by only 3 days.

Assuming a value of 63° (Díaz Trigo et al. 2006) for the inclination and a distance of 3.2 kpc (Tingay et al. 1995), the disk normalization factor (in fits made only with a power-law model plus a multicolor absorbed disk) gives inner disk radii ⁴ of 16.5 ± 0.2 km for the second epoch (the first epoch was in a hard state and had no significant contribution from the disk, as shown in Section 4.1.1). Since $R_g = 10.4$ km is the value of the gravitational radius for a $7M_\odot$ black hole, we find that the matter arrives at inner radii of $\approx 1.6R_g$ in the second epoch. This value is consistent with the value predicted for a maximally rotating black hole as explained in Section 1 ($R_{ISCO} = 1.25 R_g$) and is similar to that obtained by Tomsick et al. (1999). Analyzing *RXTE* data, Tomsick et al. (1999) found inner radii values of $R_{in} = 10.9_{-2.6}^{+2.6} - 21.9_{-5.2}^{+5.2}$ km, depending on the value adopted for the disk inclination. Of course, values of the inner disk radius inferred from any continuum fits are suspect, and must be viewed with caution. A number of effects (Merloni et al. 2000) can serve to distort the observed inner disk parameters (see Saito et al. (2007) for a determination of more realistic values for the radii, since these are not affected by a strong power-law component). According to Merloni et al. (2000), the dominant effect seems to be that the opacity is dominated by electron scattering rather than free-free absorption. The net result is that the derived temperature given by the kT_{in} parameter overestimates the effective inner temperature by a factor of 1.7 or more (Shimura & Takahara 1995).

The most interesting issue regarding our INTEGRAL observations of GRO J1655–40 is undoubtedly the presence of very significant and unbroken high energy emission up to 500 keV

⁴This radii are measured from infinity, using the formula:

$$R_{in} = D \times (diskbb_{norm} / \cos(i))^{0.5}$$

Where R_{in} is in km and D is in units of 10 kpc. This formula is inferred without taking into account gravitational effects from the General Relativity Theory. If gravitational corrections would be taken into account, then smaller co-moving radius would be obtained.

in the hard state of GRO J1655-40, as noticed from first epoch. Grove et al. (1998) made a comparative measurement of a number of systems with CGRO/OSSE and found that these systems showed a cut-off at high energies at around ~ 100 keV in the hard state of many systems ⁵. Since then several studies have tried to measure the cut-off in the spectra that could manifest the validity of Comptonization processes by thermal electrons playing the major role in the high energy emission of black holes in the hard state. In our work we did not find such a break and the presence of a non-thermal population of relativistic electrons was inferred from the fitting of our spectrum in the hard state.

Our finding is that non-thermal processes are the most important in order to explain the high energy emission of the hard state of GRO J1655-40. Additionally, there is not any break in the data indicating that the high energy emission is mainly produced by thermal Comptonization as previously claimed. Moreover, non-thermal Comptonization is the main source of the high energy emission in the second epoch (thermal dominant state). This condition for the thermal dominant state has been broadly reported in the literature since Grove et al. (1998).

In Table 3 we summarize a list of references showing breaks in the high energy emission of several black hole candidates in the hard and the intermediate state. One contemporaneous study by Shaposhnikov et al. (2006) in the hard state of GRO J1655-40 used INTEGRAL observations covering a period of time slightly prior to that of our first epoch. They pointed out the presence of a cut-off in their data at around 200 keV in their ISGRI and SPI spectra, as a manifestation of the role of thermal Comptonization being the main source of the high energy emission. However, their sensitivity at energies $\gtrsim 200$ keV is not high enough in order to disentangle the energy emission of a non-thermal population of electrons. As also noticed by Coppi (1999), if a spectrum extends up to 500 keV high energy emission coming from a non-thermal population of electrons is clearly present. The finding of the contribution of the non-thermal population of electrons in the high energy emission was reported before for the Cyg X-1 system (Malzac et al (2006), Cadolle et al. (2006) both in the intermediate state) and may be for the GRS 1915+105 (Zdziarski et al. (2001), Rodriguez et al. (2004) both in the thermal dominant state). With our study, we extend the list of sources showing high energy emission coming from non-thermal electrons with GRO J1655-40, this time in the hard state. Joinet et al. (2006) also reported the detection of a non-thermal population of electrons in the hard state of GX 339-4. However, they indicated also the presence of a cut-off in the spectra.

⁵CGRO/OSSE integration times were very long (of order of weeks), so different states would be mixed. This is not an issue for INTEGRAL, since exposures for each obtained spectrum are around two days and it is not hoped to have noticeable high energy evolution with this timing, as inferred from the light curves.

In Table 3 it can be seen that while some cut-offs appear to be close to the upper boundaries of the high energy instruments used, others appear to be physically meaningful. The last correspond to the systems GX 339-4 and Cyg X-1, both systems with known low inclination angle of $i \approx 45^\circ$ and $i \approx 35^\circ$, respectively. GRO J1655-40 is a very high inclination system with an inner disk that could have an inclination of $i = 85^\circ$ (see Section 1). Comptonization processes of soft photons through thermal and/or non-thermal electrons seems to be highly isotropical from an observer external to the system, if the electrons do not acquire outflow velocities $v/c \gtrsim 0.2$, (Beloborodov 1998), so in principle it would not depend on the inclination angle of the system. But other processes, like reflection, could depend on the view angle, being almost unobserved for high inclination systems like GRO J1655 -40 (as pointed out above with our fitting of epoch 3). So, GRO J1655-40 in the hard state would be an excellent source for the studying of Comptonization processes, without the apparent disturbance of any other high energy mechanisms (including soft emission from a disk). If these hypothesis are correct, we would have discovered that Comptonization of black hole transients in the hard state occurs by mainly Comptonization through non-thermal relativistic electrons. This conclusion is also supported by the studies of Malzac et al (2006) of Cyg X-1 in the intermediate state because while showing a high energy cut-off at the energy around 100 keV, they also point out to the presence of high energy emission from a non-thermal population of electrons in an state close to the hard (in the case of Joinet et al. (2006) in the hard state of GX 339-4).

We thank Danny Steeghs for helpful discussions. We also thank the RXTE instrument teams at MIT and NASA/GSFC for providing the ASM light curve. MDCG is a MEC funded PhD student supported under grants PNE2003-04352+ESP2005-07714-C03-03. This work is based on observations made with INTEGRAL, an ESA science mission with instruments and science data centre funded by ESA member states and with the participation of Russia and the USA. We thank to K. Arnaud for providing part of the eqpair code used in this work. We finally thank the anonymous referee for the careful reading of this manuscript.

REFERENCES

- Arnaud, K. A., 1996, ADASS, 5, 17A
- Bailyn, C. D., Orosz, J. A., Girard, T. M., Sharda, J., della Valle, M. et al., 1995, Nature, 374, 701
- Bailyn, C. D., Orosz, J. A., McClintock, J. E. & Remillard, R. A., 1995, Nature, 378, 157

- Bardeen, J. M., Press, W. H. & Teukolsky, S. A., 1972, *ApJ*, 178 ,347B
- Beloborodov, A., M., 1998, *ApJL*, 510, 123
- Borozdin, K., Revnivtsev, M., Trudolyubov, S., Shrader, C. & Titarchuk, L., 1999, *ApJ*, 517, 367
- Brockopp, C. , McGowan, K. E., Krimm, H., Godet, O., Roming, P., et al. 2006, *MNRAS*, 365, 1203B
- Michelle Buxton, Charles Bailyn, Dipankar Maitra, 2005, *ATel* 418
- Buxton, M. & Bailyn, C., 2005, *ATel* 485
- Cadolle Bel, M., Sizun, P., Goldwurm, A., Rodriguez, J., Laurent, P., Zdziarski, A. A., 2006, *A&A*, 446, 591C
- Coppi, P. S., 2000, *Bulletin of the American Astronomical Society*, 32, 1217
- Chernyakova, M., 2005, *ISDC/OSA-UM-IBIS*
- Chernyakova, M., Kretschmar, P., JEM-X team, Neronov, A., 2005, *ISDC/OSA-UM-JEMX*
- Courvoisier, T. J.-L., Walter, R., Beckmann, V., et al., 2003, *A&A*, 411, L53
- Deluit, S., (2005) *SPI-NS-0-4307-CESR*
- Díaz Trigo, M., Parmar, A., N., Miller, J. M., Kuulkers, E., Caballero-García, 2006, *astro-ph/0610873*
- Domingo, A., Caballero, M. D., Figueras, F., Jordi, C., Torra, J., Mas-Hesse, J. M., Giménez, A., Hudcova, V. & Hudec, R., 2003, *A&A*, 411, L281
- Done, C., & Nayakshin, S., 2001, *MNRAS* 328, 616
- Dubath, P., Knödlseeder, J., Skinner, G. K., Connell, P., Kreykenbohm, I., Strong, A., Sizun, P., Attié, D., Schanne, S., Cordier, B., Bouchet, L., & von Kienlin, A., 2005, *MNRAS*, 357, 420
- Ebisawa, K., Titarchuk, L. & Chakrabarti, S. K., 1996, *PASJ*, 48, 59
- Esin, A. A., McClintock, J. E., Drake, J. J. et al., 2001, *ApJ*, 555, 483
- Fender, R. P. and Belloni, T. M. & Gallo, E., 2004, *MNRAS*, 355, 1105

- Foellmi, C., Depagne, E., Dall, T. H. & Mirabel, I. F., 2006, astro-ph/0606269
- Frontera, F., Amati, L., Zdziarski, A. A. et al., 2003, ApJ, 592, 1110
- George, I. M., Fabian, A. C., 1991, MNRAS, 249, 352
- Ghisellini, G., Haardt, F. and Fabian, A. C., 1993, MNRAS, 263, L9
- Gierliński, M., Zdziarski, A., Poutanen, J. et al., 1999, MNRAS, 309, 496
- Gilfanov, M., Churazov, E. & Revnivtsev, M., 2000, Proceedings of 5-th Sino-German workshop on Astrophysics, 1999, Eds. Gang Zhao, Jun-Jie Wang, Hong Mei Qiu and Gerhard Boerner, SGSC Conference Series, vol.1, pp.114-123, astro-ph/0002415
- Goldwurm, A., David, P. & Foschini et al., 2003, A&A, 411L, 223G
- Greene, Bailyn & Orosz 2001, ApJ, 554, 1290
- Grenier, J., 1996, A&A, 120, 239
- Grenier, J., Predehl, P. & Pohl, M., 1995, A&A, 297, L67
- Grove, J. E., Strickman, M. S., Matz, S. M., Hua, X.-M., Kazanas, D. & Titarchuk, L., 1998, ApJ, 502L, 45G
- Grove, J. E., Johnson, W. N., Kroeger, R. A. et al., 1998, ApJ, 500, 899
- Hameury, J.-M., Lasota, J.-P., McClintock, J. E. & Narayan, R., 1997, ApJ, 489, 234
- Hjellming, R. M., & Rupen, M. P., 1995, Nature, 375, 464
- Homan, J. & Belloni, T. M., 2005, in From X-ray Binaries to Quasars: Black Hole Accretion on All Mass Scales, ed. T. J. Maccarone, R. P., Fender, L. C., Ho (Dordrecht: Kluwer) (astro-ph/0412597)
- Homan, J., 2005, ATel 440
- Homan et al., 2007, (in prep.)
- Ibragimov, A. Poutanen, J. Gilfanov, M., et al., 2005, MNRAS, 362, 1435I
- Joinet, A. Jourdain, E., Malzac, J., Roques, J. P., et al., 2006, astro-ph/0611064
- Kubota, A., Makishima, K., & Ebisawa, K., 2001, ApJ, 560, L147

- Kuulkers, E., Wijnands, R., Belloni, T., Mendez, M., van der Klis, M. & van Paradijs, J., 1998, *ApJ*, 794, 753
- Kuulkers, E., Shaw, S., E., Paizis, A., Chevenez, J. et al., 2007, *astro-ph/0701244*
- Laor, A., 1991, *ApJ*, 376, 90
- Lasota, J.-P., 2001, *New Astr Rev*, 45, 449
- Lebrun, F., Leray, J. P., Lavocat, P., et al., 2003, *A&A*, 411, L141
- Lubiński, P., Dubath, P., Paltani, S. et al., 2005, INTEGRAL cross-calibration status for OSA 5.1, ISDC/CCR 1.0
- Lund, N., Budtz-Jorgensen, C., Westergaard, N. J., et al., 2003, *A&A*, 411, L231
- Malzac, J., Petrucci, P.O. Jourdain, E., Cadolle Bel, M., Sizun, P., Pooley, G. et al., 2006, *A&A*, 448, 1125M
- McConnell, M. L. Ryan, J. M. Collmar, W. et al., 2000, *ApJ*, 543, 928M
- McConnell, M. L. Zdziarski, A. A. Bennett, K. et al., 2002, *ApJ*, 572, 984M
- Miller, J. M., Raymond, J., Fabian, A., Steeghs, D., et al., 2006, *Nat*, 441, 953
- Magdziarz, P. & Zdziarski, A. A., 1995, *MNRAS*, 273, 837
- Markwardt, C. & Swank, J., (2005), *ATel* 414
- Mas-Hesse, J. M., Giménez, A., Culhane, J. L., et al., 2003, *A&A*, 411, L261-L268
- Markoff, S., Falcke, H. & Fender, R., 2001, *A&A*, 372, 25
- Markoff, S., Nowak, M., Corbel, S., Fender, R. & Falcke, H., 2003, *A&A*, 397, 645
- Markoff, S., Nowak, M. A. Wilms, J., 2005, *ApJ*, 635, 1203
- Merloni, A., Fabian, A. C. & Ross, R. R., 2000, *MNRAS*, 313, 193
- Miller, J. M., Fabian, A. C., Nowak, M. A., & Lewin, W. H. G., 2005, in the Proceedings of the Tenth Marcel Grossman Meeting, Rio de Janeiro, Brazil, eds. M. novello, S. Perez Bergliaffa, & R. Ruffini, World Scientific Publishing, Singapore
- Mitsuda, K., Inoue, H., Koyama, K., et al., 1984, *PASJ* 36, 741-759
- Narayan, R. (1996), *ApJ* 462, 136-141

- Nowak, M., A., 1995, PASP, 107, 1207
- Orosz, J. A., Bailyn, C. D., 1997, ApJ, 477, 876
- Orosz, J. A., Remillard, R. A., Bailyn, C. D., & McClintock, J. E., 1997, ApJ, 478, L83
- Pottschmidt, K. Wilms, J. Chernyakova, M. Nowak, M. A. & Rodriguez, J., 2003, A&A, 411, 383
- Remillard, R. A. & McClintock, J. E, 2006, ARA&A, 44, 49
- Rodriguez, J., Fuchs, Y., Hannikainen, D., Vilhu, O., Shaw, S., 2004, ESA SP-552, 377
- Roming, P. W. A. et al., 2005, Space Reviews in press (astro-ph/0507413)
- Roques, J-P., Jourdain, E., 2005, SPI-NS-0-4305-CESR
- Roques, J-P., Jourdain, E. & Shrader, C., 2005, SPI-NS-0-4308-CESR
- M.P. Rupen (NRAO/GSFC), V. Dhawan, A.J. Mioduszewski (NRAO), 2005, ATel 419
- M.P. Rupen (NRAO/GSFC), V. Dhawan, A.J. Mioduszewski (NRAO), 2005, ATel 489
- Saito, K., Homan, J., Yamaoka, K., Fukuyama, M., 2007, astro-ph/0702022
- Shakura, N. I. and Sunyaev, R. A., 1973, A&A 24, 337-366
- Shapiro, S. L. and Teukolsky, S. A., 1983, Black Holes, White Dwarfs and Neutron Stars: The Physics of Compact Objects (Wiley, New York)
- Shaposhnikov, N., Swank, J. H., shrader, C. R. et al., 2006, astro-ph/0609757
- Shimura, T. & Takahara, F., 1995, ApJ, 445, 780
- Skinner, G. & Connell, P., 2003, A&A, 411, L123
- Sobczak, G., J., McClintock, J., E., Remillard, R. A. et al., 1999, ApJ, 520, 776
- Strohmayer, T. E., 2001, ApJ, 552, L49
- Thorne, K. S., 1974, ApJ, 191, 507T
- Tingay, S. J., et al., 1995, Nature, 374, 141
- Titarchuk, L., 1994, ApJ, 434, 570
- Titarchuk, L. & Shrader, C. R., 2002, ApJ, 567, 1057

- Tomsick, J. A., Kaaret, P., Kroeger, R. A. & Remillard, R. A., 1999, *ApJ*, 512, 892
- M.A.P. Torres (CfA), D. Steeghs (CfA), P. Jonker (SRON), P. Martini (CfA), 2005, *ATel* 417
- Ueda, Y., Inoue, H., Tanaka, Y., et al., 1998, *ApJ*, 492, 782
- Ubertini, P., Bazzano, A., Capitanio, F., De Cesare, G., 2005, *ScienceDirect*, 38, 1369
- van der Hooft, F., Heemskerk, M. H. M., Alberts, F., & van Paradijs, J., 1998, *A&A*, 329, 538
- van der Hooft, F., Kouveliotou, C., van Paradijs, J., Paciesas, W. S., Lewin, W. H. G., van der Klis, M., et al., 1999, *ApJ*, 513, 477V
- Vedrenne, G., Roques, J. P., Schönfelder, V., 2003, *A&A*, 411, L63
- Westergaard, N. J., Kretschmar, P. & Oxborrow et al., 2003, 411L, 257W
- Yuan, F. & Zdziarski, A. A., 2004, *MNRAS*, 354, 953
- Zdziarski, A. A., Grove, J. E., Poutanen, J., Rao, A. R., 2001, *ApJ*, 554, L45
- Zdziarski, A. A., Gierliński, M., Rao, A. R., Vadawale, S. V. & Mikołajewska, J., 2005, *MNRAS*, 360, 825
- Zdziarski, A. A., Gierliński, M., et al. 2004, *MNRAS*, 351, 791
- Zhang, S. N., Wilson, C. A., Harmon, B. A., Fishman, G. J., Wilson, R. B., Paciesas, W. S., Scott, M., & Rubin, B. C., 1994, *IAU Circ.* 6209

Table 1. INTEGRAL observing ToO during which GRO J1655-40 was observed in the 2005 outburst, giving the exposure times of the summed spectra analyzed for each ToO and instrument.

Epoch number	INTEGRAL revolution & MJD	Start & End Date	JEM-X	ISGRI	SPI
	(days)	(yyyy/mm/dd)	[s]	[s]	[s]
1	290 53428.20-53429.50	2005/02/27-28	44504.83	69212.87	90849.58
2	295-296 53445.10-53447.80	2005/03/16-18	43641.93	71827.16	92584.05
3	299 53455.80-53457.00	2005/03/26-28	44673.42	69848.25	—
4	304 53470.00-53471.33	2005/04/10-11	46037.85	67883.58	—

Table 2. Parameters obtained for the best fits of the joint JEM-X, ISGRI and SPI spectra (see text for details), using the model *constant* \times *eqpair* in the first epoch, *constant* \times *phabs*(*diskbb* + *eqpair*) in the second epoch, *constant* \times *phabs*(*diskbb* + *gaussian* + *pexriv*)*edge* \times *edge* in the third epoch and *constant* \times *phabs*(*diskbb* + *gaussian* + *powerlaw*)*edge* \times *edge* in the fourth epoch.

Parameter	Epoch 1	Epoch 2	Epoch 3	Epoch 4
		Powerlaw		
Γ	—	—	—	4.7 ± 0.6
N_{pow} [ph/keV/s/cm ²] at 1 keV	—	—	—	580 ± 60
		eqpair		
Γ_{p}	0.6 ± 0.3	≈ 0	—	—
γ_{min}	1.3 (f)	1.3 (f)	—	—
γ_{max}	1000 (f)	1000 (f)	—	—
l_s	10 (f)	10 (f)	—	—
l_h/l_s	0.8 ± 0.3	1.2 ± 0.6	—	—
l_{nth}/l_h	0.8 ± 0.1	0.2 ± 0.3	—	—
τ	1 ± 0.5	4 ± 1	—	—
Refl [$\Omega/2\pi$]	0(f)	0 (f)	—	—
kT_{in} (keV)	0.5(f)	1.25 ± 0.02	—	—
R_{in} (keV) [GM/c ²]	6 (f)	6 (f)	—	—
R_{out} (keV) [GM/c ²]	100 (f)	100 (f)	—	—
		diskbb		
kT_{in} [keV]	—	1.25 ± 0.02	1.28 ± 0.02	1.27 ± 0.17
N_{bb} [(R_{in} [km]/D[10kpc]) ² $\times\cos\theta$]	—	1321^{+72}_{-67}	710 ± 40	500 ± 60
		gaussian		
E_{gauss} [keV]	—	—	6.7 ± 0.3	6.7 ± 0.9
σ [keV]	—	—	0.63 ± 0.15	0.8 ± 0.5
N_{gauss} [ph/cm ² /s]	—	—	0.017 ± 0.008	0.05 ± 0.03
		edge (Fe XXV)		
E_{edge} [keV]	—	—	8.64 ± 0.20	8.6 ± 0.9
τ	—	—	0.20 ± 0.05	0.20 ± 0.10
		edge (Fe XXVI)		
E_{edge} [keV]	—	—	9.278 (f)	9.278 (f)

Table 2—Continued

	Epoch 1	Epoch 2	Epoch 3	Epoch 4
τ	—	—	≤ 0.02 (f)	≤ 0.02 (f)
Photon index	—	pexriv	2.50 ± 0.23	—
E_f [keV]	—	—	1000.0 (f)	—
R [$\Omega/2\pi$]	—	—	≤ 0.30	—
Fe abundance	—	—	2.8 (f)	—
$\cos(i)$	—	—	0.45 (f)	—
T_{disk} [K]	—	—	$1.2\text{E}+07$ (f)	—
ξ [$4\pi F_{\text{irr}}/n$]	—	—	5000 (f)	—
N_{pexriv} [ph/keV/cm ² /s]	—	—	3.8 ± 1.5	—
Instrumental normalization factors				
$C_{\text{JEM-X}}$	1.0 (f)	1.0 (f)	1.0 (f)	1.0 (f)
C_{ISGRI}	1.1 ± 0.1	1.0 ± 0.1	$0.46^{+0.11}_{-0.15}$	0.39 ± 0.14
C_{SPI}	1.4 ± 0.1	1.1 ± 0.1	—	—
χ^2_ν	1.21	1.44	2.62	2.73
ν	57	83	19	22

Note. — Parameters fixed in the fits are denoted by 'f'. We fixed the value of the column density to $N_H = 8.0 \times 10^{21}$ atoms/cm² as obtained by Díaz Trigo et al. (2006) using XMM-Newton data of GRO J1655–40 during the same outburst.

Table 3. Values for the components of Comptonization models in previous studies of several sources in several states close to the hard (LH means hard state and IS means intermediate state). Also, values for the high-energy cut-offs and/or break energies (if present) are reported.

Γ	State	$E_{cut-off}$ (keV)	E_{max} (keV)	T_e (keV)	τ	Source	Reference
1.67 ± 0.06	LH	195 ± 50	≈ 200	35_{-9}^{+200}	$1.45_{-1.4}^{+0.5}$	IGR J17497–2821	Walter et al. 2007, A&A, 461, L17
$1.4 - 1.6$	LH	$50 - 200$	≈ 200	—	—	GX 339–4	Miyakawa et al. 2007, astro-ph/0702087
1.70 ± 0.01	LH	115 ± 5.6		—	—	XTE J1550–564	Yuan et al. 2006, astro-ph/0608552
1.53 ± 0.1	LH	460 ± 300		—	—	XTE J1550–564	Yuan et al. 2006, astro-ph/0608552
1.92 ± 0.05	IS	72 ± 8	≈ 200	—	—	GX 339–4	Belloni et al. 2006, MNRAS, 367, 1113
1.9 ± 0.1	LH	≈ 150	≈ 600	67_{-6}^{+8}	1.98 ± 0.22	Cyg X-1	Cadolle Bell et al. 2006, A&A, 446, 591
2.1	IS	≈ 100	≈ 1000	$20 - 65$	$0.55 - 1.36$	Cyg X-1	Malzac et al., 2006, A&A, 448, 1125
$1.65 - 2.0$	LS	$130 - 250$	≈ 150	—	—	Cyg X–1	Wilms et al. 2006, A&A, 447, 245
1.35 ± 0.03	LH	$100 - 200$	≈ 600			GRO J1655–40	Shaposhnikov et al., 2006, astro-ph/0609757
1.72 ± 0.03	LH	—	≈ 500	—		GRO J1655–40	This work

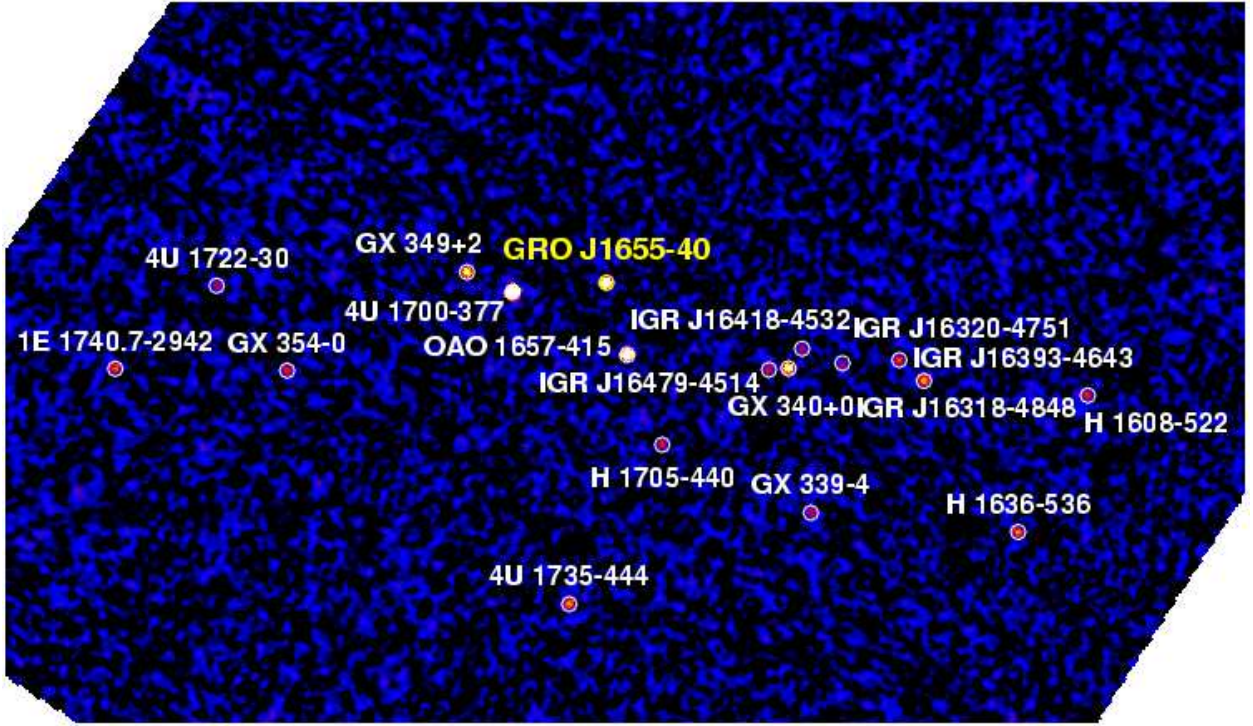


Fig. 1.— Mosaic significance image (obtained in revolution 295) of the GRO J1655-40 region as seen with ISGRI in the 20 – 40 keV energy range. Besides the target source, several other high energy sources are visible.

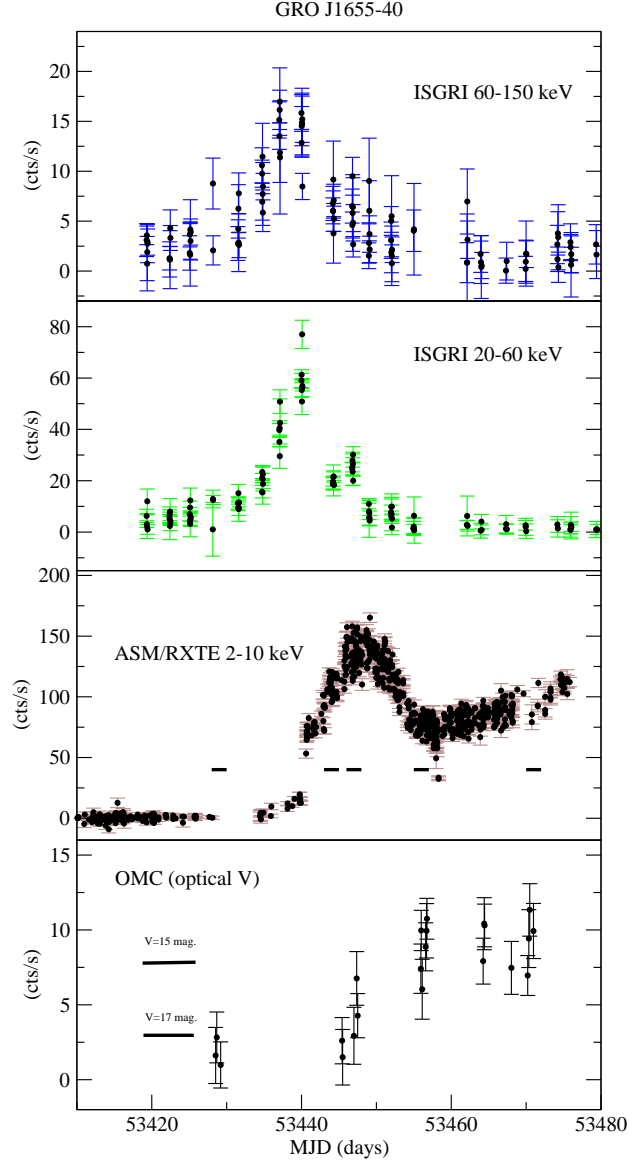


Fig. 2.— Light curves obtained with ISGRI from the INTEGRAL Galactic Monitoring Program in two energy bands (60-150 keV and 20-60 keV), together with OMC (optical). The horizontal lines in the OMC panel show the equivalence in magnitudes of the fluxes. In the third panel, ASM/RXTE (2-12 keV) light curve is shown in the same period of time. The horizontal lines indicate the time intervals (one revolution each) over which INTEGRAL spectra were obtained.

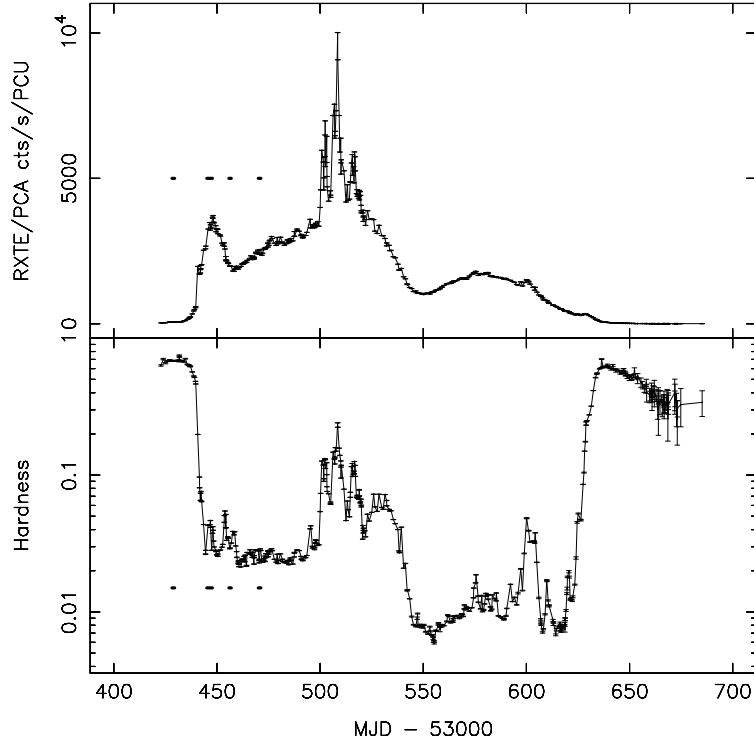


Fig. 3.— RXTE/PCA light curves in the 2-60 keV band and hardness ratio calculated as the ratio of the 9.4-18.2 keV and 2.8-5.7 keV count rates. The curves were made from 520 RXTE observations, with one (averaged) data point from each observation. Data taken from Homan et al. (2007).

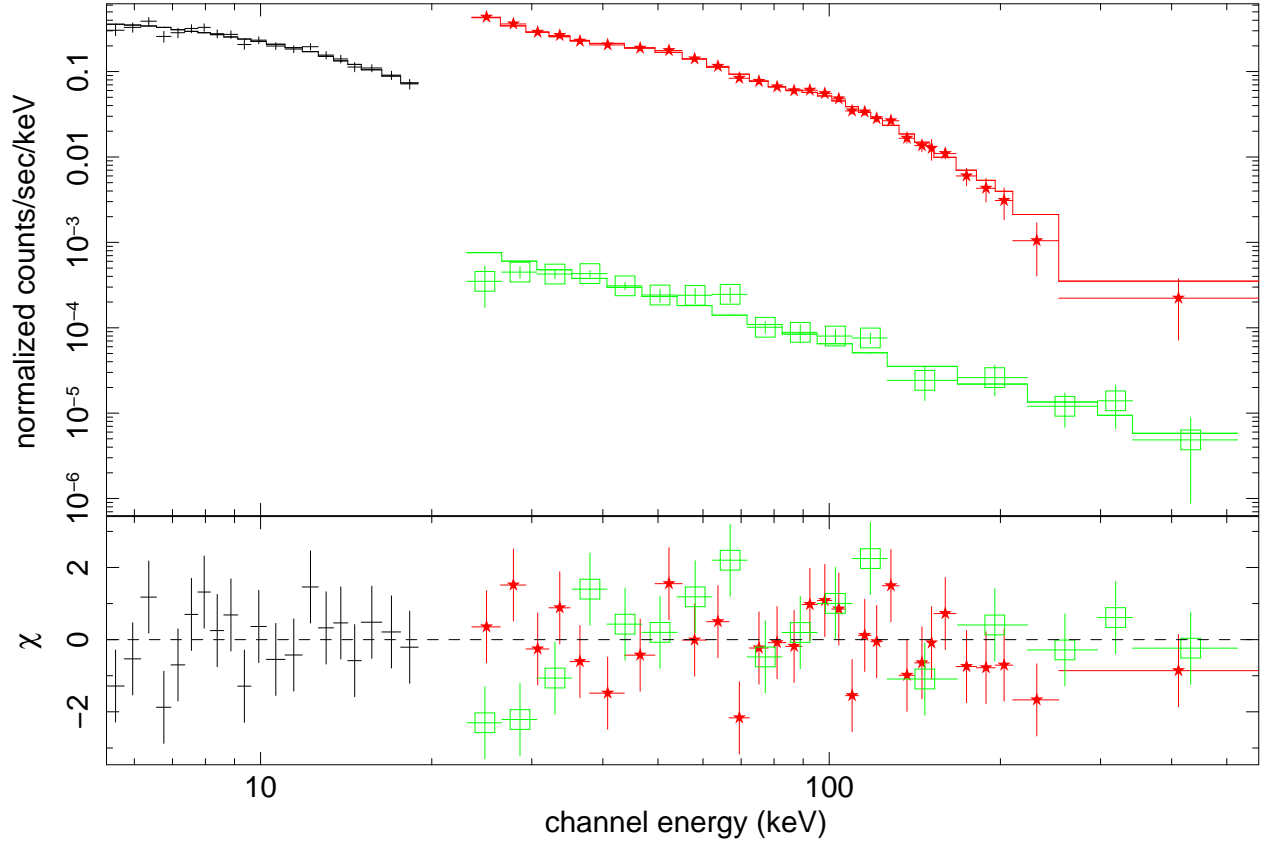


Fig. 4.— Fitted INTEGRAL spectra, corresponding to epoch 1 with a simple phenomenological power-law model. Refer to the text in Section 4.1.1 and 4.1.3 in order to get detailed information about this fit.

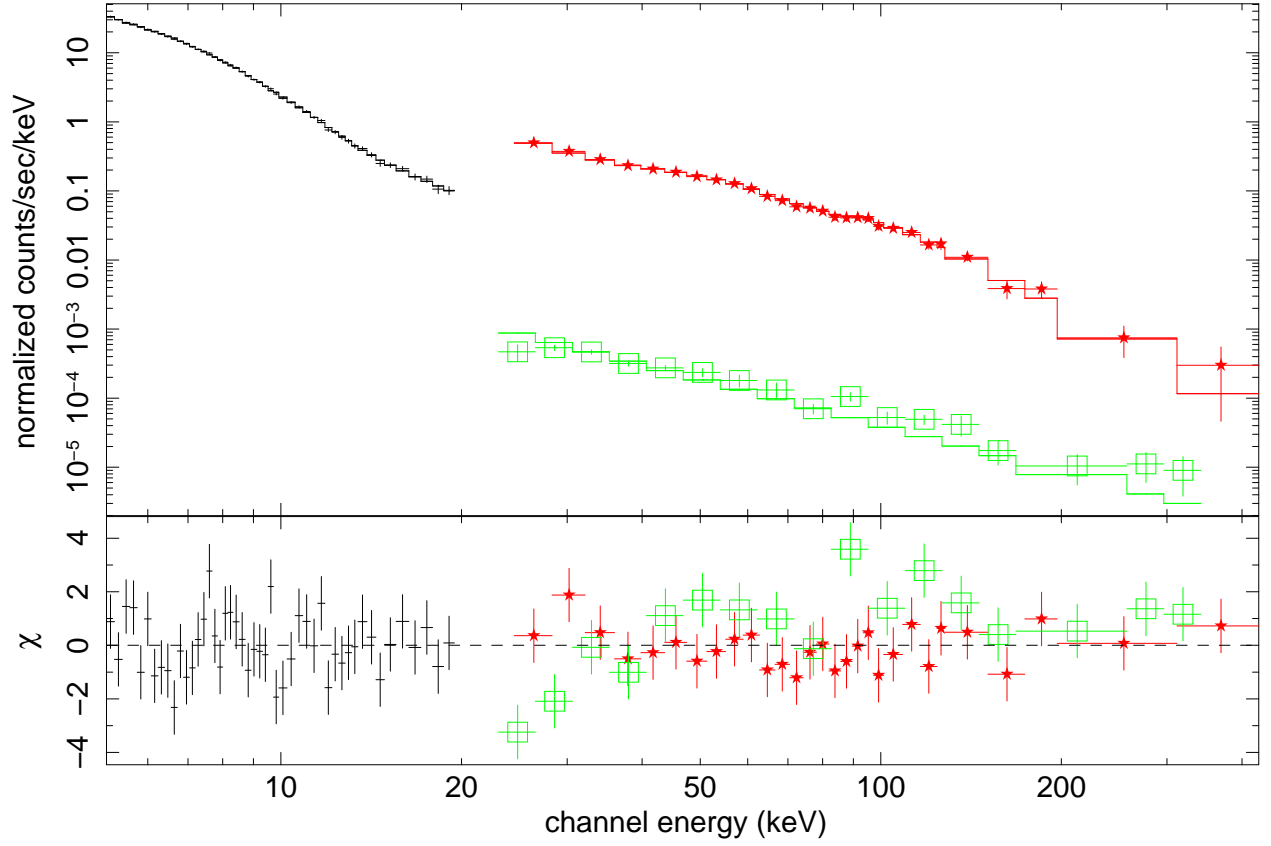


Fig. 5.— Fitted INTEGRAL spectra, corresponding to epoch 2 with a simple phenomenological power-law model. Refer to the text in Section 4.1.1 and 4.1.3 in order to get detailed information about this fit.

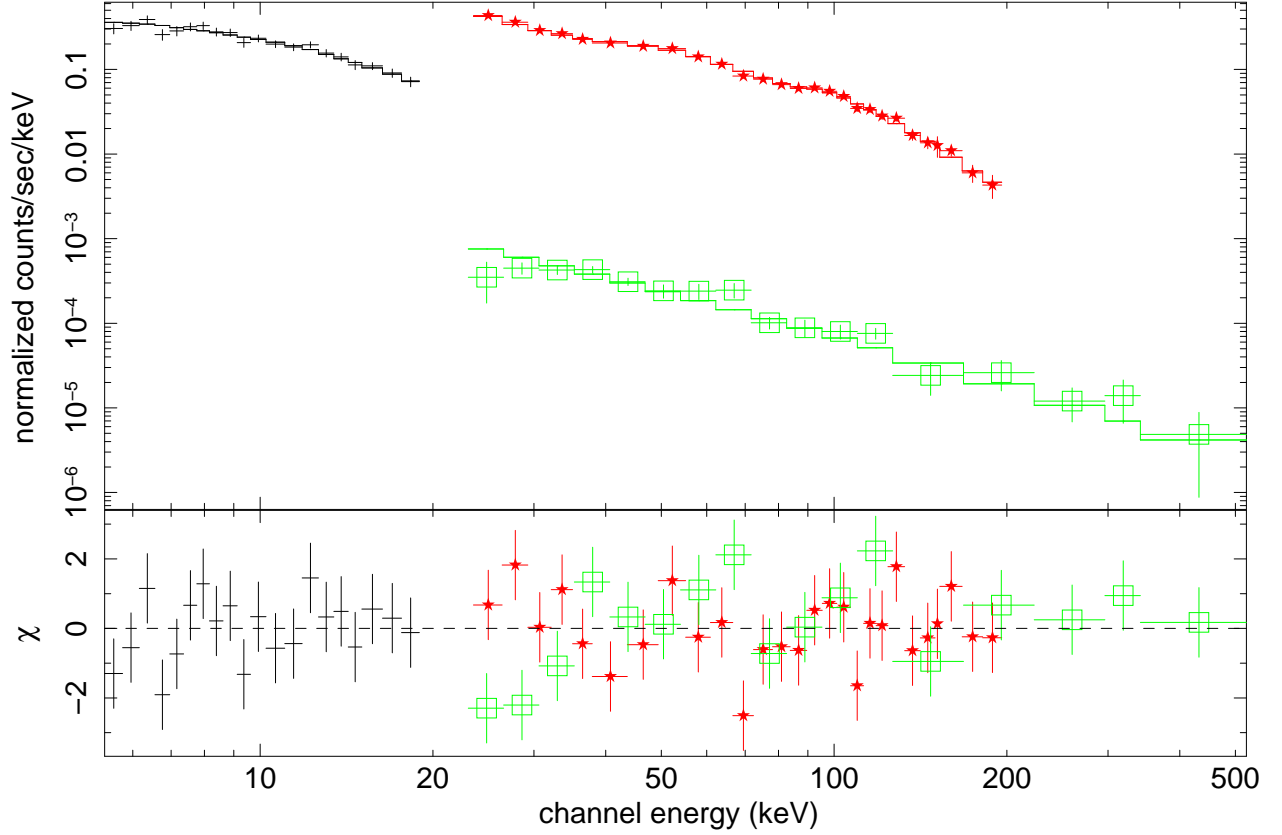


Fig. 6.— Fitted INTEGRAL spectra, corresponding to epoch 1 (hard state). These spectra were fitted with the EQPAIR Comptonization model of Coppi (1999) (*eqpair* model in XSPEC). Details about the fitting and the parameters obtained in Section 4.1.2 and in Table 2. JEM-X (single line -black-), ISGRI (star line -red-) and SPI spectra (square line -green-), are shown, respectively.

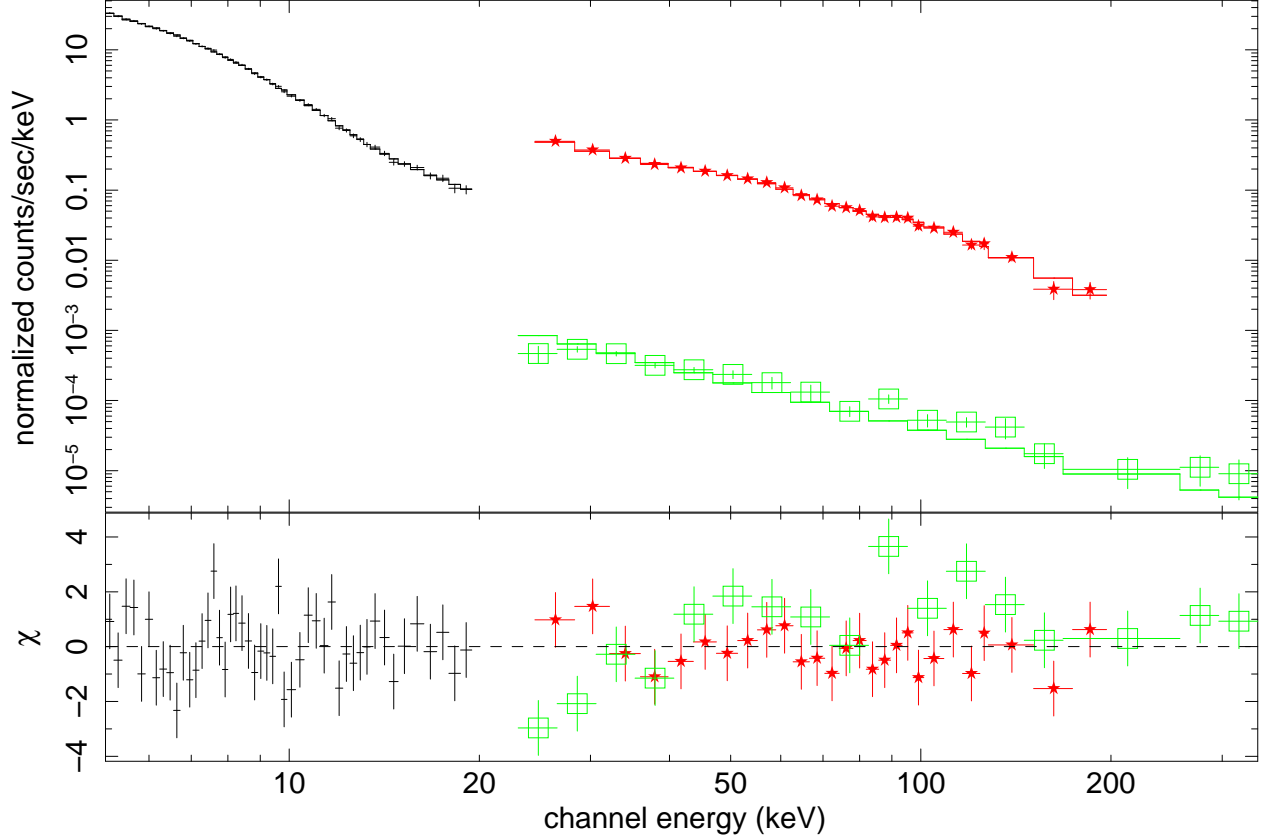


Fig. 7.— Fitted INTEGRAL spectra, corresponding to epoch 2 (thermal dominant state). These spectra were fitted with the EQPAIR Comptonization model of Coppi (1999) (*eqpair* model in XSPEC) considering also the soft emission from an accretion disk (*diskbb* model in XSPEC). Details about the fitting and the parameters obtained in Section 4.1.2 and in Table 2. JEM-X (single line -black-), ISGRI (star line -red-) and SPI spectra (square line -green-), are shown, respectively.

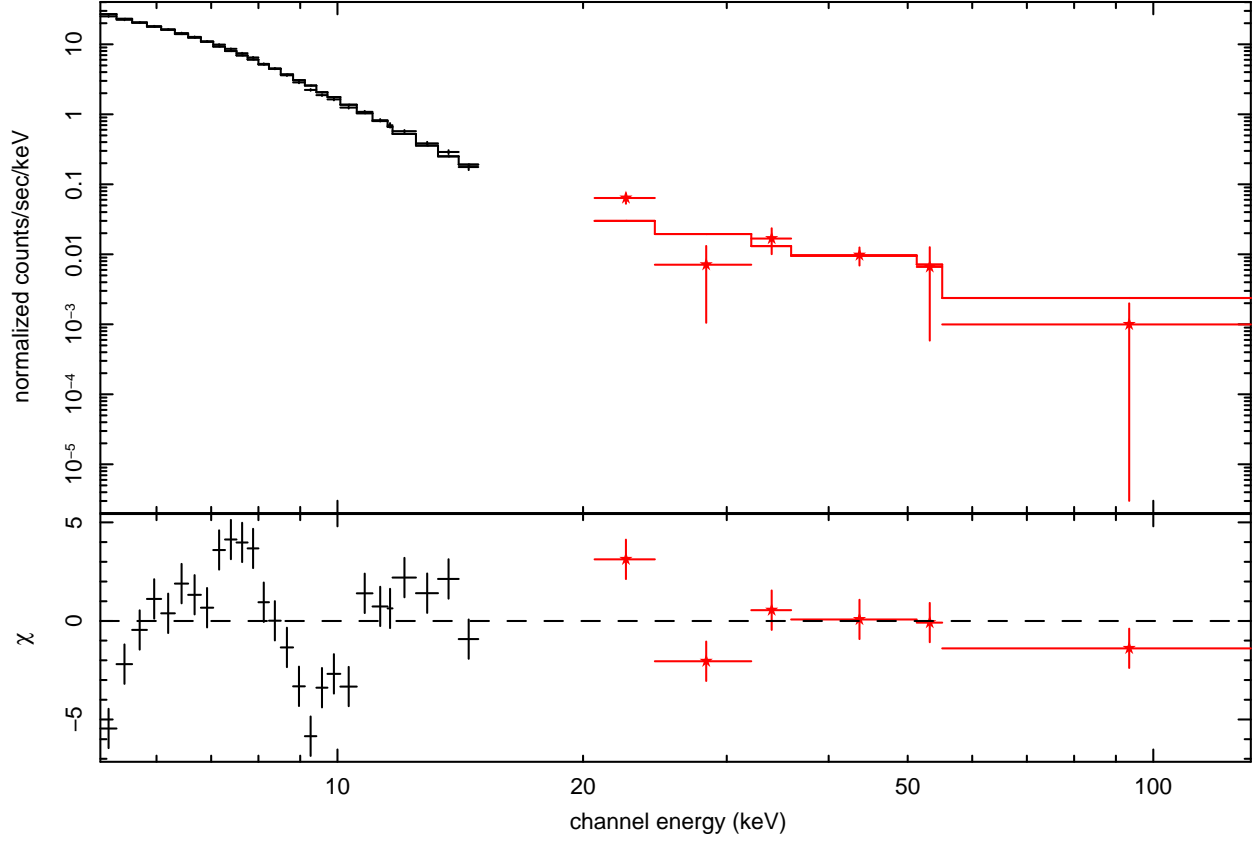


Fig. 8.— Fitted INTEGRAL spectra, corresponding to epoch 4 (thermal dominant state). The model used was one consisted of a pure power-law plus emission from an absorbed multicolor accretion disk of Mitsuda et al. (1984). In this period we noticed a change in the properties of the accretion outflow with respect to epochs 1 and 2 (see Section 4.1.1 and 5 for details).

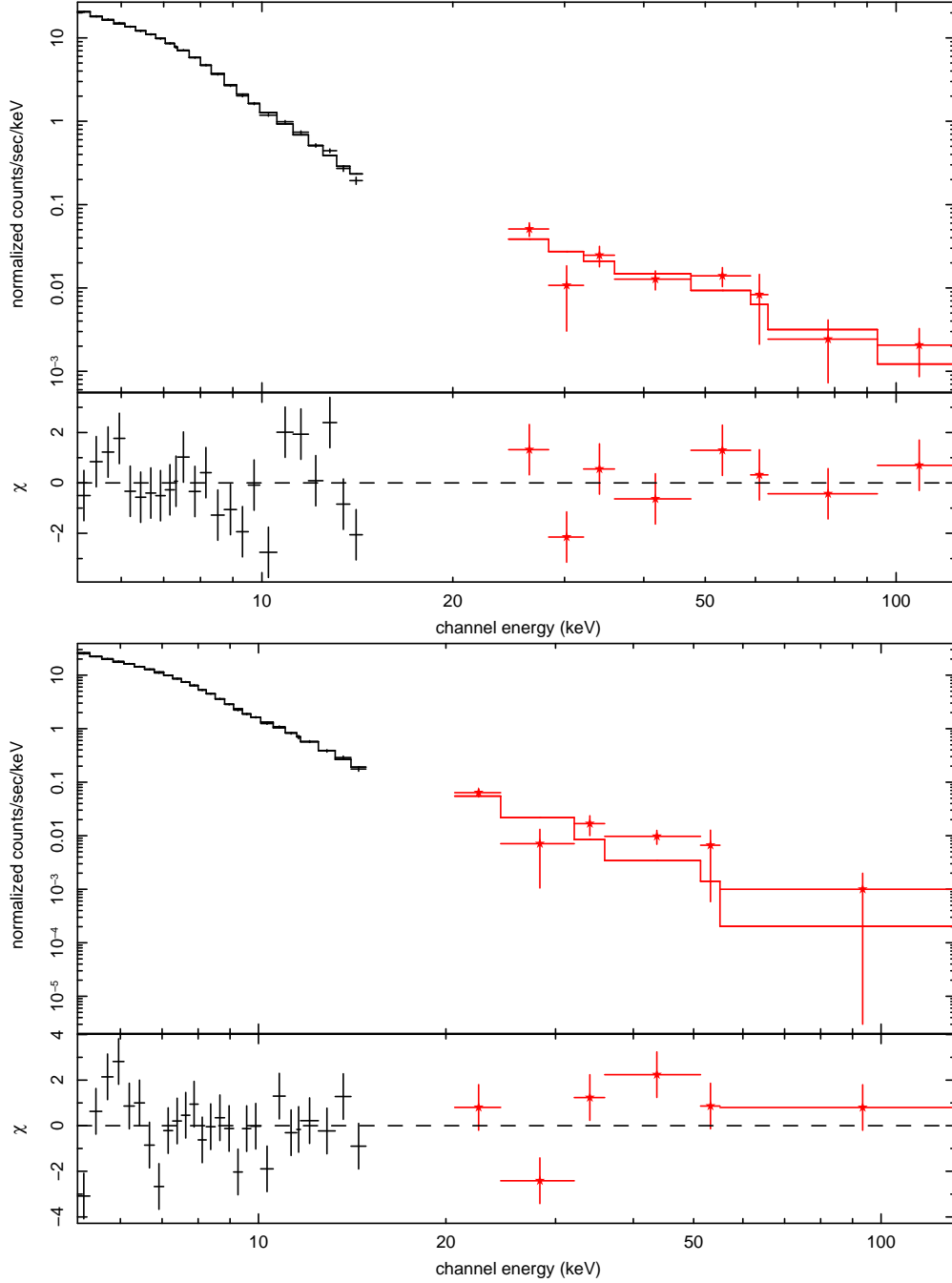


Fig. 9.— Fitted INTEGRAL spectra, corresponding to epochs from 3 and 4 (upper to lower panel). These spectra were fitted with an absorbed multicolor disk (Mitsuda et al. 1984) plus a simple power-law iron emission line and edges for both two epochs (and reflection in the case of epoch 3). Details about the fitting and the values of the parameters obtained in Section 4.2 and Table 2. JEM-X (single line -black-) and ISGRI (star line -red-) are shown, respectively.

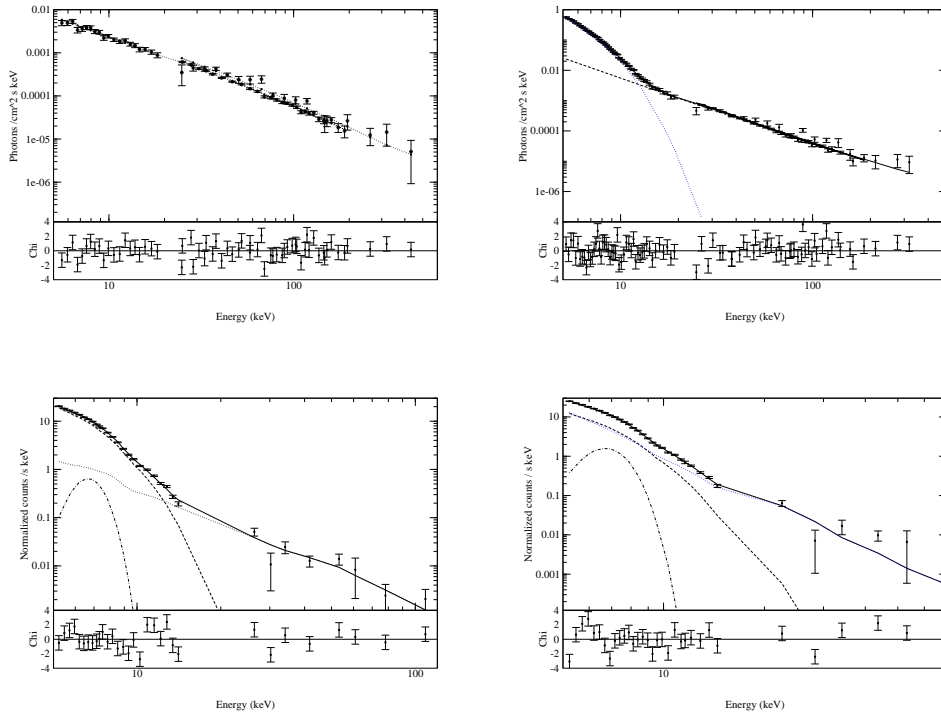


Fig. 10.— Unfolded spectra from epochs 1 to 4 (upper-left to lower-right). The continuum line shows the total model (see the text and Table 2 for details), the dashed-dotted line shows the iron $K\alpha$ emission line, the long dashed line the accretion disk component and the short dashed line the power-law (*pexriv* in the third epoch).